Mine Water and the Environment (2021) 40:877–890
https://doi.org/10.1007/s10230-021-00821-y

TECHNICAL ARTICLE

Control of Water-Flowing Fracture Development with Solid Backfill Mining: Designing a Backfill Body Compression Ratio for Water Resources Protection

Yun Zhang[1,2] **· Shenggen Cao**[3]

Received: 9 August 2020 / Accepted: 27 August 2021 / Published online: 7 September 2021

Abstract
Coal development in China is shifting to its ecologically-vulnerable western regions where the loss of water resources is a major problem with respect to protecting the ecological environment. The results of physical similarity simulation tests showed that the movement and deformation of the strata above the stope with cave mining created a 'domino effect', which caused further interconnected fractures and loss of water resources. On that basis, we propose the use of solid backfill mining (SBM) to actively control the development of water-flowing fractures. Moreover, a mechanical model describing the development of water-flowing fractures in the overlying strata under SBM was established, the evaluation criteria and method were defined, and the variation rule of the height of water-flowing fractured zone with the backfill body compression ratio was derived. Finally, a case study was performed in an experimental coal mine in Shaanxi. After engineering the design, the minimum critical backfill body compression ratio corresponding to no water resource loss with SBM was calculated to be 21.3%. The field measured data (103.7 m) was very consistent with the results of the mechanical calculation (106.9 m), verifying the accuracy and reliability of the mechanical model. This research can help protect water resources and further enhance coal recovery.

Keywords Mechanical model · Environmental protection · Water-flowing fractured zone · Aquifer · Protective layer

Introduction

The development of China's coal resources has rapidly shifted to its western regions. Coal reserves in western China now account for more than 85% of the country's total (Chi et al. 2019; Fan 2018; Zhang et al. 2020). However, the western coal mines are mostly located in deserts and desert edges that have severe water shortages, sparse surface vegetation, soil erosion, and fragile ecological environments (Shan et al. 2020; Zhang et al. 2011). Water resources play a decisive role in maintaining local industrial and agricultural development and ecological balance. During the coal mining process, the overlying strata above the stope undergoes intensive movement and large-scale damage, which inevitably cause rock caving and produce fractures. Once these fractures are interconnected, water channels form, which are also referred to as water-flowing fractured zones (Ju et al. 2020; Zhang and Shen 2004). These water channels might further trigger related environmental issues such as betrunking of streams, more serious land desertification, damage to buildings, reduced surface vegetation, and death of crops. Figure 1 displays environmental problems that were caused by coal mining. Additionally, after large-scale and extensive mining for a long time, a large amount of gangue is discharged and accumulates on the surface, which can cause pollution of soil and surface water. Furthermore, harmful gases that are produced during spontaneous combustion also create severe issues for the eco-environments of coal mines (Huang et al. 2012; Zhang et al. 2014, 2019). The government's sustainable development strategy was heavily influenced by this environmental destruction and waste of

✉ Yun Zhang
zhangyun@cumt.edu.cn

[1] School of Energy Science and Engineering, Xi'an University of Science and Technology, Xi'an 710054, Shaanxi, China

[2] Key Laboratory of Western Mines and Hazard Prevention of Ministry of Education, Xi'an University of Science and Technology, Xi'an 710054, Shaanxi, China

[3] State Key Laboratory of Coal Resources and Safe Mining, China University of Mining and Technology, Xuzhou 221116, Jiangsu, China

(a) Land desertification (b) Damage to buildings (c) Fractures reach to surface

Fig. 1 Environment damages were caused by coal mining in China

coal resources. Accordingly, this study proposes the use of solid backfill mining (SBM) for recovering coal seams under an aquifer, both to address the accumulation of gangue on the surface and to control the development of water-flowing fractures and rock strata movement.

Scholars have conducted a considerable amount of theoretical research on water-saving coal mining. Fan et al. (2015, 2017) reviewed the latest development and the existing scientific problems regarding water-saving mining at different phases in ecologically fragile mining areas of western China. Zhang et al. (2010, 2017a) proposed the short-wall cave mining method to save water when mining under hard-thick strata. To resolve the conflict between water conservation and coal mining, Ma et al. (2015) proposed a water-saving mining technique for long-wall working faces with an emphasis on rapid advancement of the working face. Xu et al. (2009, 2012) analyzed the influencing rules of the key strata of overlying strata on the development height of the water-flowing fractured zone and proposed a new method for estimating the height of the water-flowing fractured zone based on the position of the key strata. Pu (2008, 2010) proposed the concept of water-resisting key strata and carried out a systematic analysis of the fracture distribution characteristics of water-resisting key strata. Scheiber et al. (2018) proposed a method for managing groundwater and observing changes of the groundwater levels in mining sites according to multivariate statistical analysis, which could determine groundwater loss after mining.

For SBM with gangue, Miao et al. (2010) proposed the mechanism, method, and related mining systems and devices for backfilling with gangue. By analyzing the correlation between the compaction deformation of gangue backfill body and time, Zhang et al. (2015, 2016) proposed the equivalent mining height model. Huang et al. (2012, 2020) started from strata control, analyzed the influence of the backfill body (gangue materials) on the backfill body compression ratio, and thereby proposed a method to design the backfill body compression ratio of the working face based on the compaction characteristics of the backfill body. Sun et al. (2017) proposed longwall roadway backfill coal mining, and analyzed the characteristics of the overlying strata movement and optimization of roadway size. To evaluate the effect of strata control by SBM, Li et al. (2017) proposed the backfill body compression ratio as the technical index to analyze the main factors of the backfill body compression ratio. Yan et al. (2019) analyzed the characteristics of overlying strata displacement of ultra-contiguous coal seams under different backfill body compression ratios, and then optimized the ratio for ultra-contiguous coal seams. Huang et al. (2019) analyzed the physical and mechanical characteristics of five backfill materials (aeolian sand, gangue, mineral waste residue, coal ash, and loess) and found that the stress increase rate is faster with aeolian sand. Hence, aeolian sand provides support for the roof more effectively and quickly. Deng et al. (2020) proposed the microbial mixed SBM method, and studied the effects of various factors on the mechanical properties of backfill materials of microbial mixed SBM. Qi et al. (2019) investigated the behavior of contaminative metal ions in the gangue using static immersion tests, and found that the concentration and diffusion distance of contaminative metal ions increased over time, which was negatively correlated with gangue particle size. However, the development of water-flowing fractures in the overlying strata under an aquifer using SBM has rarely been investigated thus far and needed further research.

Therefore, this study focused on an experimental coal mine in Yan'an, Shaanxi, and analyzed the effect of the cave mining method on water loss through physical similarity simulation tests. SBM was proposed for recovering the coal seams under the aquifer and a mechanical model of a superposition beam with an elastic foundation was established for describing the development of water-flowing fractures in the overlying strata under SBM conditions. We also theoretically analyzed the minimum critical backfill body compression ratio for ensuring no water loss during the SBM process. The present study has important engineering and reference significance for further enhancing the coal recovery ratio, ecological/environmental protection, and reasonable recovery of coal seams under the aquifer.

Engineering Background

The experimental coal mine is located in the northeastern part of the Huanglong Jurassic coalfield, Yan'an, Shaanxi. The coal mine field covers an area of ≈ 197.5 km^2 with an east-to-west length of ≈ 13 km and a south-to-north width of

≈ 23 km. The approved comprehensive production capacity was 4.2 Mt/a. Currently, the primary mineable coal seam is the #2 coal seam, which has a mean thickness of ≈ 4.0 m and a mean inclination of 2.0°. Hence, the #2 coal seam can be regarded as horizontal.

Based on hydrogeological conditions, the aquifer in the coalfield is the surface water from local branches of the largest river on the surface. The river, which has a length of 100 km, and covers an area of 3392 km^2 is the main potentially protected water resource in the mining area. The observed river discharge ranges from 0.584 to 11.111 m^3/s. Locally, the coal seam has a shallow burial depth. To avoid water loss, the east side of the no. 402 working face, where the coal seam had a simple and stable structure and no faults, was set as the experimental SBM working face. The mean coal seam thickness was ≈ 4.0 m and the strike length of the experimental working face was ≈ 250 m. Surface rivers were located above the loess layer and were ≈ 141.6 m from the coal seam. Figure 2 shows the location of the experimental SBM working face and the geological composition of the roof strata, based on the nearby S81 drill hole.

Analysis of the Mechanisms of Water Resources Loss Under Cave Mining

Establishment of the Physical Similarity Model

This study focused on the experimental SBM working face of a coal mine in Yan'an, Shaanxi, which had typical regional mining geological conditions. The surface water loss mechanism during the cave mining process was investigated by analyzing the movement and deformation behaviors of the overlying strata and the development of water-flowing fractures in a physical similarity simulation test. According to physical similarity criteria and field geological structure, the prototype and the physical similarity model should satisfy the following similarity conditions: the similarity ratio of bulk density was 1:1.667, the similarity ratio of geometry was 1:150, and the similarity ratio of stress and strength was 1:250. Finally, a plane strain model of 2.5 m × 0.2 m × 0.99 m was established, and a physical similarity model was constructed using sand, calcium carbonate, gypsum, and water. The physical similarity model included 13 layers from the floor to the surface. The floor under the coal seam was composed of a 3.0 m thick layer of sandy mudstone. During paving of each layer from the bottom to top, sand, calcium carbonate, gypsum, and water were stirred in an agitator according to the similarity material proportions (Table 1). After stirring, the materials were evenly placed on the model support and tamped with a specially-made hammer until the height of each layer reached the designed height. Mica sheets ≤ 1 mm were laid between the adjacent layers.

It should be noted that the sand used in the physical similarity simulation test contained a certain amount of water since problems that would reduce the accuracy of the physical similarity simulation test, such as low proportions and high humidity, could be induced if the moisture content of the sand was ignored (Zhang 2019). Therefore, it was necessary to adjust the material proportions as shown in Table 1. Meanwhile, six different 250 g sand samples were tested before model construction and then baked in a drying oven until the water was completely removed. After drying, the

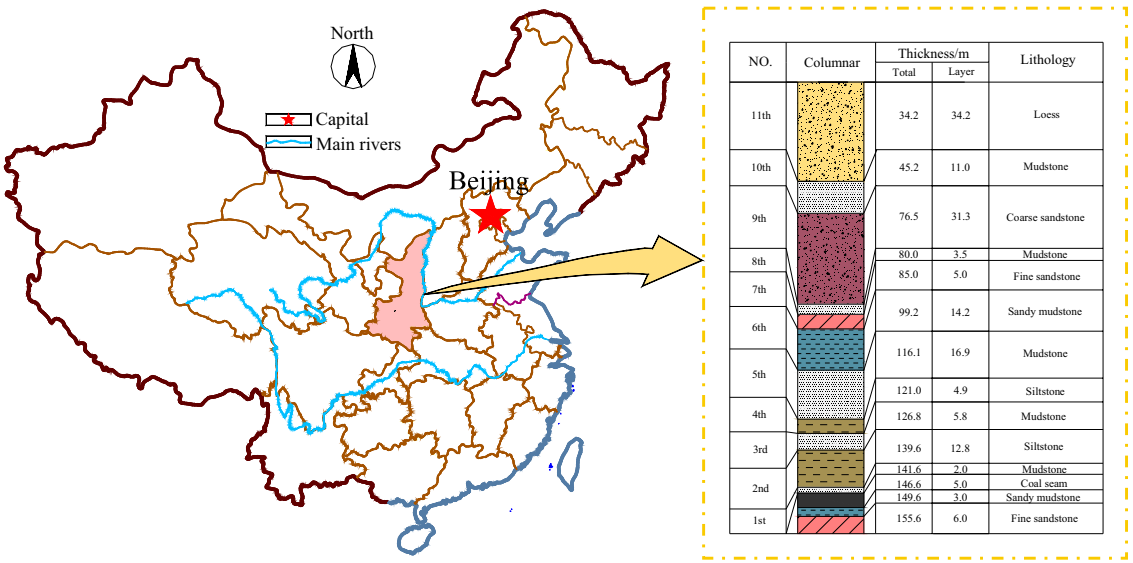

Fig. 2 Location and geologic column above the coal seam of experimental solid backfill mining (SBM) working face

Table 1 Ratio parameters of materials for physical similarity simulation test

	Lithology	Thickness/m	Simulated thickness/cm	Simulated strength/kPa	Sand/kg	Calcium carbonate/kg	Gypsum/kg	Water/kg
1	Loess	34.2	22.8	0.2	179.55	17.96	7.69	22.8
2	Mudstone	11.0	7.3	70.0	57.49	5.75	2.46	7.3
3	Coarse sandstone	31.3	20.9	174.4	161.23	8.06	18.81	20.9
4	Mudstone	3.5	2.2	70.0	17.33	1.73	0.74	2.2
5	Fine sandstone	5.0	3.3	202.0	22.28	3.71	3.71	3.3
6	Sandy mudstone	14.2	9.5	103.2	74.81	5.34	5.34	9.5
7	Mudstone	16.9	11.3	70.0	89.0	8.9	3.8	11.3
8	Siltstone	4.9	3.3	180.0	25.46	1.27	2.97	3.3
9	Mudstone	5.8	3.9	70.0	30.71	3.07	1.32	3.9
10	Siltstone	12.8	8.5	180.0	65.57	3.28	7.65	8.5
11	Mudstone	2.0	1.3	70.0	10.24	1.02	0.44	1.3
12	Coal seam	4.0	2.6	63.2	20.48	2.05	0.87	2.6
13	Sandy sandstone	3.0	2.0	129.2	15.75	0.68	1.57	2.0

sand was weighed. Supplemental Figure S-1 compares the sand samples before and after drying. Supplemental Figure S-2 shows the masses of the six sand samples before and after drying. The moisture content of each sand sample, which was denoted as ψ, were then calculated using Eq. (1):

$$\psi = \frac{m_s - m_g}{m_s} \tag{1}$$

where m_s denoted the mass of sand before drying and m_g denoted the mass of sand after drying. The moisture content of the sand samples were calculated and averaged as the final data (4.65%).

Since the moisture content of the sand used in the physical similarity simulation test was 4.65%, the actual amount of sand should be greater than the value in Table 1 in the physical similarity model. The weight of the required water-bearing sand was adjusted according to the following equation:

$$m_s' = \frac{m_s}{(1-\psi)} \tag{2}$$

where m_s' denoted the mass of the required water-bearing sand after model correction, and m_s denoted the mass of the required dry sand before model correction in Table 1.

Clearly, the weight of water in the physical similarity model had to be reduced. The weight of the required water in the physical similarity model was calculated as:

$$m_w' = m_w - m_s' \times \psi \tag{3}$$

where m_w' denoted the mass of the required water after model correction, and m_w denoted the mass of the required water before model correction in Table 1.

The weights of sand and water as well as the moisture content of the sand listed in Table 1 were then substituted into Eqs. (2) and (3), and the proportions of the experimental materials in various strata of the model were corrected. Table 2 lists the material proportions of various strata in the corrected physical similarity model, which were used to establish the physical similarity model.

The displacement of the overlying strata and the development of water-flowing fractures were monitored. After model construction and air drying, marks were sprayed onto the model surface, and the displacement was monitored using the Vic 2D noncontact full-field strain measurement system. Using the digital image correlation (DIC) operational rules, Vic 2D can realize displacement and deformation measurements in a 2-dimensional view field. Fig. 3 displays the model monitoring process.

During the physical similarity simulation test, the drying degree of the model decisively affected the physical properties. This study used a 20.9 m thick layer of fine sandstone; 60 cylindrical samples were prepared with a height of 100 mm and a diameter of 50 mm. These samples and the physical similarity model were cured under the same environment (Fig. 4b). Due to the low strength of the samples during the early stage, the testing was started 7 days after the samples were finished curing. Figure 4c displays the strength

Table 2 Corrected ratio parameters of materials for physical similarity simulation test

	Lithology	Thickness/m	Simulated thickness/cm	Simulated strength/kPa	Sand/kg	Calcium carbonate/kg	Gypsum/kg	Water/kg
1	Loess	34.2	22.8	0.2	188.31	17.96	7.69	14.04
2	Mudstone	11.0	7.3	70.0	60.29	5.75	2.46	4.5
3	Coarse sandstone	31.3	20.9	174.4	169.09	8.06	18.81	13.04
4	Mudstone	3.5	2.2	70.0	18.17	1.73	0.74	1.36
5	Fine sandstone	5.0	3.3	202.0	23.37	3.71	3.71	2.21
6	Sandy mudstone	14.2	9.5	103.2	78.46	5.34	5.34	5.85
7	Mudstone	16.9	11.3	70.0	93.34	8.9	3.8	6.96
8	Siltstone	4.9	3.3	180.0	26.7	1.27	2.97	2.06
9	Mudstone	5.8	3.9	70.0	32.21	3.07	1.32	2.4
10	Siltstone	12.8	8.5	180.0	68.77	3.28	7.65	5.3
11	Mudstone	2.0	1.3	70.0	10.74	1.02	0.44	0.8
12	Coal seam	4.0	2.6	63.2	21.48	2.05	0.87	1.6
13	Sandy sandstone	3.0	2.0	129.2	16.52	0.68	1.57	1.23

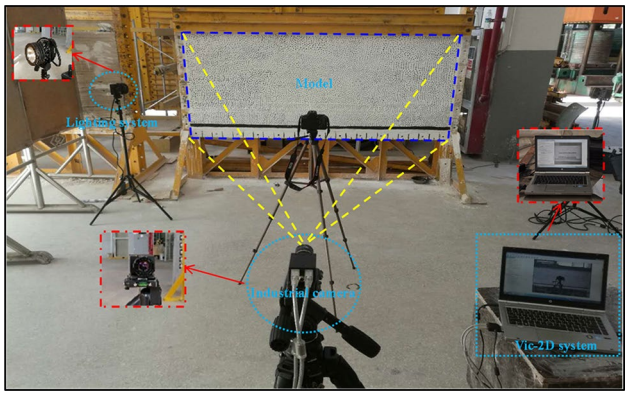

Fig. 3 Model and monitoring system

characteristics of the samples over time. After 18 days, the compressive strength of the samples (200 kPa) was almost equal to the simulated value of the fine sandstone. Therefore, the physical similarity model was excavated 18 days after it was established.

Analysis of the Test Results

Movement and Deformation Characteristics of the Overlying Strata

Figure 5 displays the vertical deformation cloud chart of the overlying strata by cave mining through the Vic-2D non-contact strain monitoring system. After the coal seams in the mining region were excavated using the cave mining method, the balance of the initial rock stress was destroyed. Consequently, the roof was deformed and broke, layer by layer from bottom to top. Due to the large volume of the gob, the basic roof and main key strata broke, and the overlying strata exhibited synchronous coordinated motion overall. This resulted in serious subsidence and deformation on the surface. The maximum subsidence of the surface was ≈ 21.2 mm in the physical similarity model. Moreover, the vertical displacement of the overlying strata was greatest at the center above the gob and gradually dropped toward the coal mass. The maximum vertical displacement of the overlying strata above the working face was 36.0 mm.

(a) Established model (b) Environment of samples (c) Compressive strength of samples

Fig. 4 Time determination of model excavation

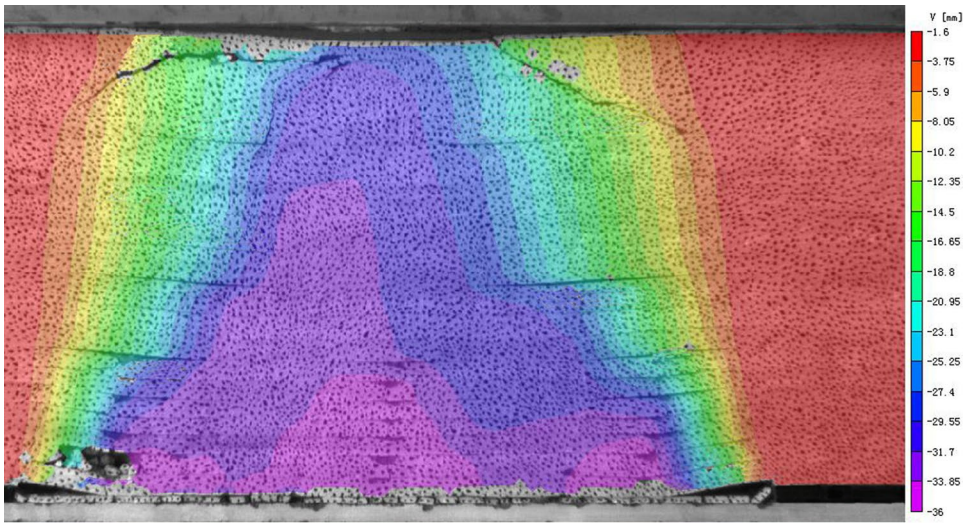

Fig. 5 Vertical deformation cloud chart of the overlying strata by cave mining

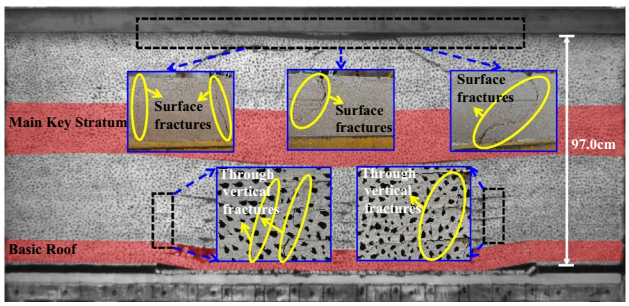

Fig. 6 Distribution of the water-flowing fractured zone by cave mining

Development of the Water-Flowing Fractures

Figure 6 displays the distribution of the water-flowing fractured zone of the overlying strata under cave mining. As shown in Fig. 6, the results of physical similarity simulation test revealed that the broken main key stratum led to overall deformation and failure of the overlying strata above the working face. Then, the water-flowing fractures developed to the surface, which triggered thin, deep transverse cracks on the surface. Accordingly, the surface exhibited slight step submergence. The height of the water-flowing fractured zone was ≈ 97.0 cm. The aquifuge was located in the fractured zone, which provided favorable conditions for water loss and destroyed the surface water layer. Furthermore, a series of environmental problems could be triggered, such as land desertification, sparse surface vegetation, and the betrunking of stream, which would thereby aggravate the contradiction between environmental protection and coal mining.

According to the movement and development characteristics of the water-flowing fractures of the overlying strata above the gob, the hanging area of the roof gradually increased as the working face advanced. Moreover, the bearing capacity of the lower levels of the overlying strata decreased, thereby inducing successive breaks from bottom to top and generating interconnected fractures. Given the bulk increase of the broken strata, the rotational deformation space of the higher level of overlying strata was small, which led to a steady drop in the displacement of the overlying strata from bottom to top. Once the main key stratum was deformed and broken, the strata above the main key stratum underwent overall deformation and failure in a 'domino effect'. It can be seen from Fig. 6 that if the mining height is too high, the strata above the stope undergoes severe deformation and failure. Also, the maximum tensile stress of the strata can exceed their tensile strength and generate interconnected fractures. This could cause the water-flowing fractures to reach the surface, leading to a loss of surface water resources. Therefore, the SBM method, which supports the overlying strata by backfilling the gangue into the gob, was proposed for recovering the coal seams under an aquifer. SBM reduces the rotational deformation space of the strata and restricts the development of water-flowing fractures.

Analysis of the Mechanical Characteristics of Water-Flowing Fractures with SBM

Movement of the Overlying Strata

After the coal seam was mined using SBM, the gangue was timely backfilled to the gob, in full contact with the roof to bear the load of the overlying strata. Accordingly, the subsidence space of the overlying strata was effectively reduced, leading to better control of strata movement and failure. This fundamentally changed the deformation characteristics of the surrounding rocks in the stope and restricted

the development of water-flowing fractures of the overlying strata. Therefore, the loss of water resources could be effectively avoided by using the SBM method. According to field measurements (Li et al. 2014; Yan et al. 2018; Zhang et al. 2014), when the backfill body compression ratio reaches a certain value, there should be only two zones above the working face, namely, the fractured zone and bending zone; no caving zone is observed. Supplemental Figure S-3 displays the movement characteristics of the overlying strata under SBM.

Establishment of a Mechanical Model of Water-Flowing Fractures Development Under SBM

After all of the operating procedures in the SBM working face were completed, the height of the water-flowing fractured zone was determined by calculating the failure height of the overlying strata above the stope based on the SBM technology and the movement characteristics of the overlying strata (Miao et al. 2011; Zhang et al. 2018). An arbitrary stratum (denoted as the eth stratum) above the stope was taken as the research object. Then, a mechanical model of superposition beam with an elastic foundation was established to describe the development of water-flowing fractures in the overlying strata along the advancing direction under SBM conditions. The load on the eth stratum could be simplified as a uniformly-distributed load $q(e)$. The eth stratum was supported by lower strata, coal mass, and backfill body, which could be simplified as the Winkler elastic foundation. The advancing length of the SBM working face, the length of backfill body was denoted by l, while h denoted the mining height of the coal seam, and h_1, h_2, h_3, …, h_j denoted the respective thicknesses of various strata above the stope. The total thickness of all strata from the 1st stratum to the eth stratum above the coal seam were calculated as $H_e = \sum h_e (e = 1,\ 2,\ 3,\ \ldots,\ j)$. $k_c{}^e$ and $k_b{}^e$ denoted the elastic foundation coefficients of the coal mass and the backfill body, respectively, and k_1, k_2, …, $k_{e\text{-}1}$ denoted the elastic foundation coefficients of the various strata below the eth stratum. Supplemental Figure S-4 illustrates the mechanical analysis of the basic environmental state of the eth stratum under SBM.

The elastic foundation coefficients of the backfill body, coal mass, and all the strata below the eth stratum could be expressed as:

$$\begin{cases} \dfrac{1}{k_c^e} = \dfrac{1}{k_c} + \dfrac{1}{k_1} + \dfrac{1}{k_2} \ldots + \dfrac{1}{k_{e-2}} + \dfrac{1}{k_{e-1}}, & \text{combination of coal mass and strata} \\ \dfrac{1}{k_b^e} = \dfrac{1}{k_b} + \dfrac{1}{k_1} + \dfrac{1}{k_2} \ldots + \dfrac{1}{k_{e-2}} + \dfrac{1}{k_{e-1}}, & \text{combination of backfill body and strata} \end{cases} \tag{4}$$

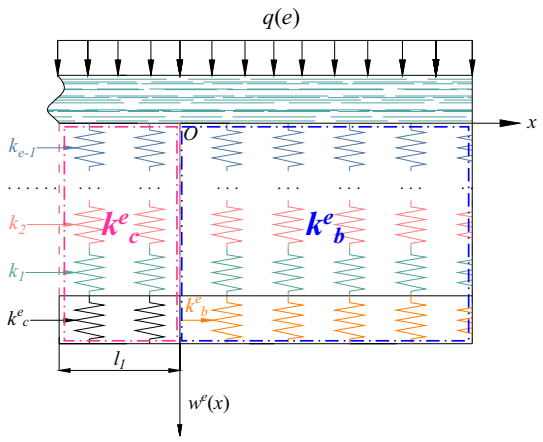

Fig. 7 Mechanical model of the eth stratum under SBM

As shown in Figure S-4, the mechanical model was a positively symmetrical structure under the environmental state. To simplifying the calculation process, half of the mechanical model was selected for further analysis. By taking the center of the SBM working face along the advancing direction as the symmetrical point, and selecting the original point O of the coal mass at the starting cut position, a mechanical coordinate system was established (Fig. 7). In Fig. 7, the displacement function $w^e(x)$ was set as the y-axis, and the advancing direction of the working face was set as the x-axis.

According to the assumption of a Winkle elastic foundation, the subsidence at any point of the foundation surface was in direct proportion to the applied pressure per unit area, which actually simulated the foundation as a series of independent springs on a rigid base. When a point on the foundation surface was subjected to pressure p, only local subsidence $w^e(x)$ was generated at that point because the springs are independent. No subsidence appeared in other regions. Thus, p could be written as:

$$\begin{cases} p_1 = k_c^e w_1^e(x), & \text{above the solid coal} \\ p_2 = k_b^e w_2^e(x), & \text{above the backfill body} \end{cases} \tag{5}$$

where p denoted the pressure per unit area and $w^e(x)$ denoted the subsidence of the foundation.

Based on the elastic foundation beam theory (Selvadurai and Gladwell 1979; Yu et al. 2016), the deflection of eth stratum and the load should satisfy the following differential equations of the deflection curve:

$$\begin{cases} E_e I_e \dfrac{d^4 w_1^e(x)}{dx^4} + p_1 = q(e) \\ E_e I_e \dfrac{d^4 w_2^e(x)}{dx^4} + p_2 = q(e) \end{cases} \tag{6}$$

where $E_e I_e$ denoted the flexural rigidity of the rock beam cross-section.

Different foundation media represented the springs with different properties. Therefore, the coal mass, the backfill body, and each stratum under the eth stratum were assumed to be mutually independent springs. Moreover, the coal mass on the left side of stope could be regarded as a semi-infinite elastic foundation. Then, the eth stratum could be regarded as a semi-infinite beam. By substituting Eq. (6) into Eq. (7), the deflection equation of the eth stratum above the coal mass and backfill body could be described as:

$$\begin{cases} \dfrac{d^4 w_1^e(x)}{dx^4} + \dfrac{k_c^e w_1^e(x)}{E_e I_e} = \dfrac{q(e)}{E_e I_e}, & (x \le 0) \\ \dfrac{d^4 w_2^e(x)}{dx^4} + \dfrac{k_b^e w_2^e(x)}{E_e I_e} = \dfrac{q(e)}{E_e I_e}, & (x \ge 0) \end{cases} \tag{7}$$

where $E_e I_e$ denoted the flexural rigidity of the eth stratum.

Eq. (7) was solved by setting the characteristic coefficients $\alpha = \sqrt[4]{\frac{k_c^e}{4E_e I_e}}$ and $\alpha = \sqrt[4]{\frac{k_c^e}{4E_e I_e}}$. Then, the deflection equation of the eth stratum could be written as:

$$\begin{cases} w_1^e(x) = \dfrac{q(e)}{k_c^e} + d_1 e^{\alpha x} \cos \alpha x + d_2 e^{\alpha x} \sin \alpha x + d_3 e^{-\alpha x} \cos \alpha x + d_4 e^{-\alpha x} \sin \alpha x, & (x \le 0) \\ w_2^e(x) = \dfrac{q(e)}{k_b^e} + d_5 e^{\beta x} \cos \beta x + d_6 e^{\beta x} \sin \beta x) + d_7 e^{-\beta x} \cos \beta x + d_8 e^{-\beta x} \sin \beta x, & (x \ge 0) \end{cases} \tag{8}$$

The elastic foundation coefficient of the backfill body and the backfill body compression ratio could be written as:

$$k_c^e = \frac{\sigma_0}{h_k(1-\varphi)} \tag{9}$$

where σ_0 denoted the initial rock stress of coal seam and φ denoted the backfill body compression ratio ($0 < \varphi < 1$) (Huang et al. 2017; Zhang et al. 2017b).

The boundary conditions of the eth stratum could be described as:

$$\begin{cases} \theta_1^e(-\infty) = 0, \ w_1^e(-\infty) = 0 \\ \theta_2^e\left(\dfrac{l}{2}\right) = 0, \ Q_1^e\left(\dfrac{l}{2}\right) = 0 \end{cases} \tag{10}$$

The continuity conditions of the eth stratum could be described as:

$$\begin{cases} \theta_1^e(0) = \theta_2^e(0), \ w_1^e(0) = w_2^e(0) \\ M_1^e(0) = M_2^e(0), \ Q_1^e(0) = Q_2^e(0) \end{cases} \tag{11}$$

The required parameters to be determined (d_1, d_2, d_3, d_4, d_5, d_6, d_7, and d_8) were obtained by substituting Eqs. (4), (9), (10), and (11) into Eq. (8). Hence, the bending subsidence equations of the eth stratum, ${w_1}^e(x)$ and ${w_2}^e(x)$, as well as the bending moment equation, ${M_1}^e(x)$ and ${M_2}^e(x)$, could be solved.

According to the theory of material mechanics, the maximum tensile stress of the eth stratum could be solved by the following equation:

$$\sigma_{\max}^e = \left| \frac{6M_{\max}^e}{h_k^2} \right| \tag{12}$$

where ${\sigma^e}_{\max}$ denoted the maximum tensile stress of the eth stratum and ${M^e}_{\max}$ denoted the maximum bending moment of the eth stratum.

Based on the first strength theory, the eth stratum generating the water-flowing fractures should satisfy the following equation:

$$\sigma_{\max}^e \ge [\sigma_e] \tag{13}$$

where $[\sigma_e]$ denoted the tensile strength of the eth stratum.

If Eq. (13) was satisfied, the stratum would break and produce water-flowing fractures; if not, no water-flowing fractures would be generated. The analysis was started from the first stratum above the coal seam. When its tensile strength was less than the maximum tensile stress, the first stratum would produce water-flowing fractures. Then, the adjacent upper stratum was checked. The calculation stopped when the tensile strength of a stratum was higher than the maximum tensile stress. Figure 8 displays the detailed method for calculating the height of the water-flowing fractured zone. The height of the water-flowing fractured zone, H, was equal to the sum of the thicknesses of various broken strata:

$$H = h_1 + h_2 + h_3 + \ldots\ldots \tag{14}$$

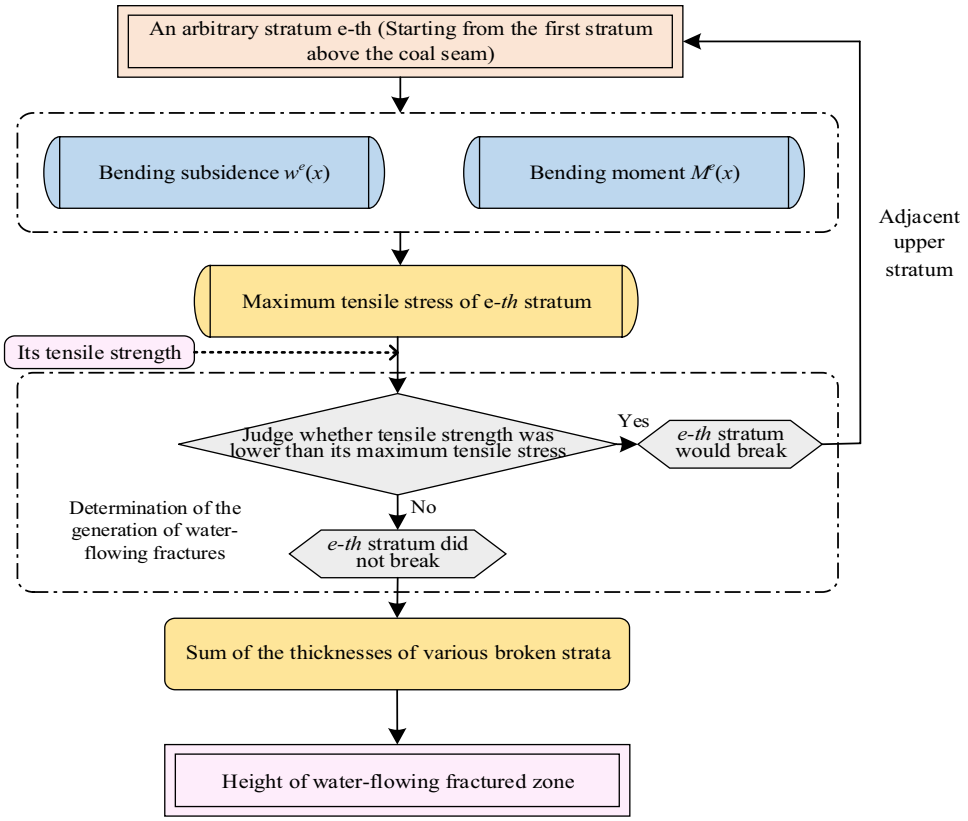

Fig. 8 Detailed method for calculating the height of the water-flowing fractured zone

Engineering of SBM for Water Resources Protection

Main Factors Influencing Water-Flowing Fracture Development with SBM

By analyzing the mechanical properties of the development of water-flowing fractures in the overlying strata under SBM, it was found that the main factors influencing the height of the water-flowing fractured zone were the mining height, backfill body compression ratio, advancing length of the working face, burial depth, thickness of the coal seam and strata, and the elasticity modulus of the coal seam and strata. However, under certain engineering geological conditions, the last four remain unchanged. Therefore, the first two are described below.

Mining Height

Mining height is an important factor that affects the destruction of the overlying strata. After coal mining, the stress around the mining space is redistributed, and stress is concentrated locally, which results in breakage of the strata. Different mining heights can generate different heights of the 'three zones' in the overlying strata. According to the predictive equation for calculating the height of the water-flowing fractured zone, the mining height is also the only factor that affects the development of water-flowing fractures, as per the *Regulation of Coal Mining under Buildings, Railways and Water Bodies* (Ministry of Emergency Management of the People's Republic of China 2017).

Backfill Body Compression Ratio

The backfill body compression ratio is the ratio of the final height of the backfill body after compaction to the mining height and is a crucial factor for maintaining the stability of the overlying strata in the stope. If the backfill body compression ratio is too low, the backfill body cannot provide effective support. Then, the strata above the working face breaks successively from bottom to top as with cave mining, which restricts the development of water-flowing fractures to a certain degree. When the backfill body compression ratio reaches a certain value, the backfill body acts as the main supporting body and restricts movement of the roof. The overlying strata mainly exhibits bending subsidence, where the water-flowing fractures only develop locally.

Design of the Critical Backfill Body Compression Ratio for Water Resource Protection

According to the condition of the coal seams in the field SBM working face, the mining height was set as 5.0 m to enhance coal recovery rates. Therefore, the engineering

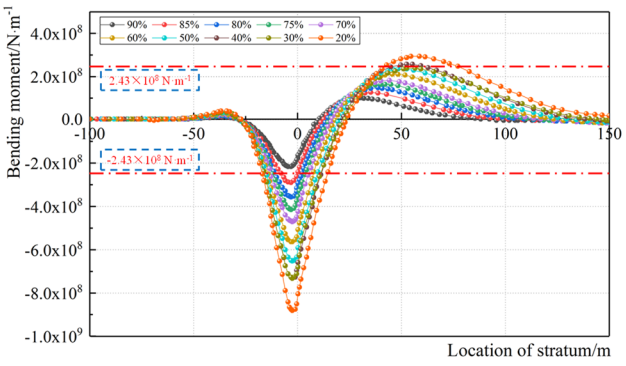

Fig. 9 Bending moment curve of siltstone with a thickness of 12.8 m at different backfill body compression ratios

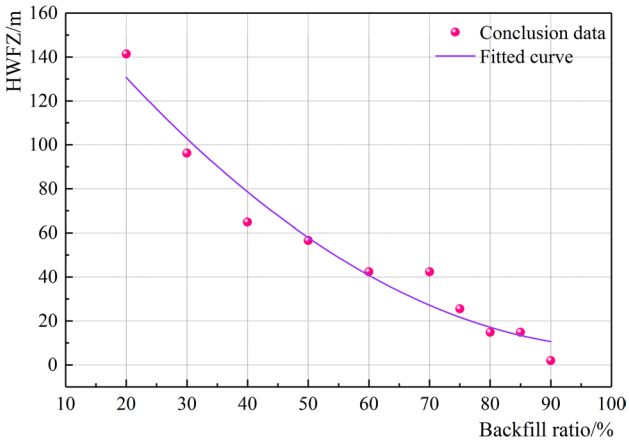

Fig. 10 Curve-fitting between height of water-flowing fractured zone and backfill body compression ratio

design of the SBM for water resources protection was being determined by the critical backfill body compression ratio. Using a 12.8 m thick siltstone with different backfill body compression ratios as an example, the related calculation parameters were substituted into the mechanical model for derivation, and the bending moment curve of the stratum was plotted (Fig. 9). The tensile strength was substituted into Eq. (12) for inversion. The absolute value of the ultimate bending moment was calculated to be 2.43×10^8 N/m. For comparison, siltstone would break and produce water-flowing fractures at a backfill body compression ratio less than 90%.

The related engineering parameters were substituted into the mechanical model. In combination with the detailed method for calculating the height of the water-flowing fractured zone, the height range of water-flowing fractured zone with respect to the backfill body compression ratio was plotted, as shown in Fig. 10.

By performing nonlinear regression on the height of the water-flowing fractured zone with different backfill body compression ratios, the predictive equation could be fitted as:

$$H = 0.02\varphi^2 - 3.6\varphi + 196.9 \quad R^2 = 0.958 \tag{15}$$

where H denoted the height of the water-flowing fractured zone, φ denoted the backfill body compression ratio, and R^2 denoted the coefficient of determination.

Obviously, Eq. (15) is only applicable to the experimental coal mine in Yan'an, Shaanxi, and other coal mines with similar geological conditions. By substituting the thickness of the constrained strata (141.6 m, the distance between the coal seam and the aquifer) into the fitted predictive equation of the height of the water-flowing fractured zone, it was calculated that a backfill body compression ratio exceeding 20% would prevent water-flowing fractures from develop to the aquifer.

Discussion

Determining the Thickness of the Protective Layer

To avoid the loss of water resources by coal mining, the *Regulation of Coal Mining under Buildings, Railways and Water Bodies* specifies that the designed minimum thickness of the water proof coal-rock pillar (denoted as H_{fmin}, i.e. the minimum distance between the mining coal seam and the aquifer) should equal the sum of the height of the water-flowing fractured zone, H, and the thickness of the effective protective layer, H_p, (see Fig. 11):

$$H_{f\,\min} = H + H_p \tag{16}$$

According to the structural characteristics and mechanical properties of the coal-rock layers in the experimental mining region (as shown in Fig. 2), the roof above the stope was medium hard strata. Therefore, based on the specifications of the thickness of the protective layer in *Regulation of Coal*

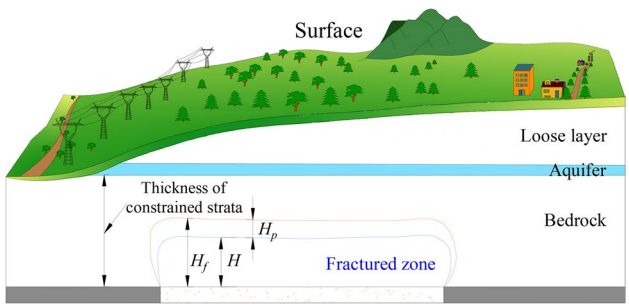

Fig. 11 Relationship between the effective protective layer and HWFZ

Mining under Buildings, Railways and Water Bodies, the thickness of the protective layer was calculated as:

$$H_p = 3h_k = 12m \tag{17}$$

By substituting Eqs. (15) and (17) into Eq. (16), the relationship between the backfill body compression ratio for water resources protection and minimum thickness of the water proof coal-rock pillar was derived as:

$$H_{f\,\min} = 0.01\varphi^2 - 3.6\varphi + 209 \tag{18}$$

By substituting the thickness of the constrained strata (141.6 m) into Eq. (18), adverse effects on water resources can be avoided at a minimum critical backfill body compression ratio of 21.3%. In addition, the backfill materials (backfill body) acts as the main support for bearing the load of the overlying strata. This effectively lowered the height of the water-flowing fractured zone and simultaneously enhanced both the upper limit and the recovery ratio of coal seam mining. Accordingly, SBM allows water-saving mining below an aquifer. The scope of using Eq. (18) and Eq. (15) is the same for the experimental coal mine in Yan'an, Shaanxi, and other coal mines with similar geological conditions.

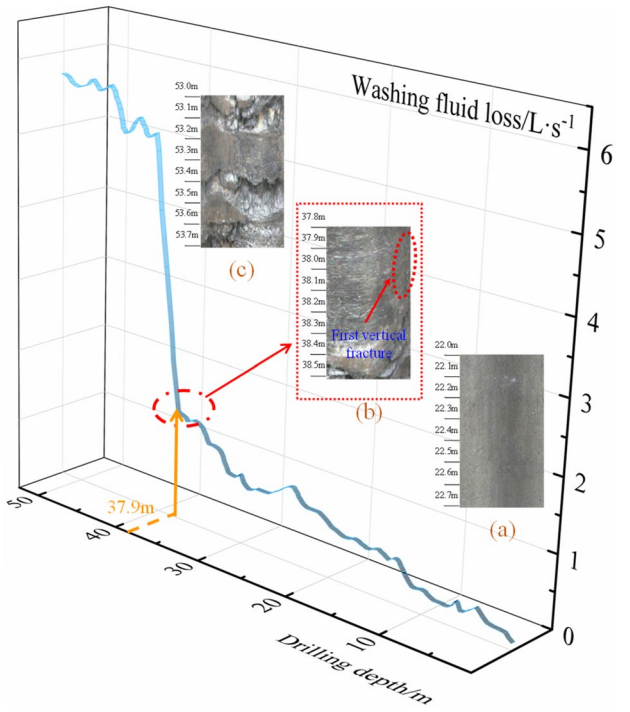

Fig. 12 The variation of the washing fluid loss and the distribution of fractures in borehole L1. **a** No fracture; **b** first vertical fracture; **c** fractured zone

Engineering Practice

To protect water resources, the backfill body compression ratio of the experimental SBM working face in the experimental coal mine was set as 30%. Three months after the mining and backfilling of the experimental SBM working face was completed, an observation borehole was drilled in the central position above the working face (borehole L1). The height of the water-flowing fractured zone was determined by observing washing fluid loss and from drillhole TV imaging. The location of borehole L1 is illustrated in Supplemental Figure S-5. The final drilled position of borehole L1 was the roof stratum of the working face. In the process of drilling, the washing fluid loss, the degree of damage to the core, and the distribution of fractures in the overlying strata were monitored.

In borehole L1, the range of the washing fluid loss and the distribution of fractures are shown in Fig. 12. When the drilling depth reached 37.9 m, the washing fluid loss increased from 0.2 to 1.53 L/s, a relatively small change. There was no obvious fracture in the core of the borehole. At the same time, it could be seen from the TV imaging that there were no fractures and that the morphology was relatively complete (Figure 12a). As the drilling depth increased, the washing fluid loss rapidly increased to 5.2 L/s, and the loss rate fluctuated greatly. Additionally, the core was relatively broken, and the fracture directions were different, with narrow widths. As shown in Fig. 12b, the top boundary of the water-conducting fractured zone and the first vertical fracture appeared at 37.9 m in borehole L1. At greater drilling depth, drill falling and seizing occurred occasionally. The washing fluid loss was stable at about 5.7 L/s, and the amount of loss varied slightly. Meanwhile, as can be seen from Fig. 12c, the density of vertical fractures of the overlying strata increased with the borehole depth. Therefore, it was determined that the top boundary of the water-flowing fractured zone was at a depth of ≈ 37.9 m in borehole L1.

According to the measured results in the field, it was determined that the height of the water-flowing fractured zone caused by SBM was about 103.7 m, and the water-flowing fractures had not developed to the surface water layer. The top boundary of the water-flowing fractured zone was about 37.9 m from the surface water layer, which was much greater than the thickness of the protective layer (12 m). Thus, SBM effectively protected the water resources in the experimental coal mine.

When the designed backfill body compression ratio (30%) of the experimental SBM working face were put into Eq. (15), theoretical analysis showed that the height of the water-flowing fractured zone was 106.9 m. Table 3 demonstrates that the measured results in the field were essentially consistent with the results of the prediction of the mechanical calculation, which confirms that the mechanical model was highly accurate and reliable. Furthermore, these findings

Table 3 Comparative analysis of the height of the water-flowing fractured zone

Height of the water-flowing fractured zone	Measured results	Prediction of the mechanical calculation
	103.7 m	106.9 m

show that SBM can play a significant role in protecting water resources.

Analysis of Economic and Environmental Benefits

Compared with cave mining, SBM better controls the movement and breakage of rock stratum through the backfill body (gangue materials). Moreover, SBM restricted the development of water-flowing fractures to the aquifer, so that the water resource would not be lost. The key to protect water resources during SBM was to control the development of water-flowing fractures by reducing strata movement. Moreover, the use of SBM prevents potential environmental problems caused by loss of water resources and surface subsidence, such as soil and water loss, soil nutrient loss, land carrying capacity decline, land desertification, surface buildings damage, sparse ground vegetation, and crop death. Furthermore, the gangue materials were backfilled into the gob, which prevented the pollution of the soil and surface water caused by gangue accumulation on surface and avoided the harmful gases produced by spontaneous combustion of the gangue.

The investment of mine geo-environmental restoration had increased in China. From 2000 to 2006, the government invested 2.4 billion yuan to remedy the mine geo-environment. In addition, the Ministry of Environmental Protection of China issued the *Technical Specifications of Eco-environmental Protection and Reclamation for Mining* in 2013, which regulated the eco-environmental protection and restoration during exploitation of mineral resources. By the end of 2014, the cumulative investment of mine geo-environmental restoration funds had reached 90.1 billion yuan (Bian et al. 2018; Hu et al. 2020). However, using SBM will allow the mining of coal seams under aquifers, which would enhance the recovery rate of coal resources and reduce the cost of coal production. Furthermore, backfilling gangue materials into the gob reduced the damage to the environment and minimized the cost of geo-environmental restoration of the coal mines. To summarize, the SBM method could effectively enhance the production rate of coal resources and the protection of water resources, thus achieving an effective balance between economic and environmental benefits.

Many encouraging policies and guidelines had been promulgated by the national government to encourage coal mines to use SBM technology in China. For example, *Gangue Comprehensive Management Measures* clearly states that gangue can no longer be accumulated on the surface (Zhou et al. 2020), so coal mines have had to spend a lot of money to deal with it. Thus, SBM could save the cost of gangue disposal for coal mines. At the same time, the resource tax of coal mines using SBM could be discounted by 50% (Liu et al. 2021). In addition, Shandong, Shanxi, and other regions have promulgated the *Incremental replacement of production capacity using SBM*, which stipulates that the actual production capacity could be increased to 3.3 times of the designed production capacity using SBM (Li 2021). In summary, it can be seen that SBM is becoming important in Chinese coal mining.

Conclusions

This study investigated the recovery of coal seams under an aquifer through the use of SBM. This approach supports the overlying strata with the backfilled gangue, which restricts the development of water-flowing fractures. By analyzing the movement of the overlying strata with SBM, a mechanical model of a superposition beam with an elastic foundation was established for describing the development of water-flowing fractures in the overlying strata under SBM conditions, and a method to calculate the height of the water-flowing fractured zone in the overlying strata was proposed. The heights of the water-flowing fractured zone in the overlying strata were calculated at different backfill body compression ratios, and the predictive equation was fitted as: $H = 0.02\varphi^2 - 3.6\varphi + 196$, which is applicable to the experimental coal mine in Yan'an, Shaanxi, and other coal mines with similar geological conditions, but would have to be modified for use elsewhere.

This study focused on the geological conditions of an experimental coal mine in Shaanxi. The minimum critical backfill body compression ratio of the experimental SBM working face based on water resources protection was determined to be 21.3%. In other words, the loss of water resources could be effectively avoided with a backfill body compression ratio that was more than 21.3%. The field measurements showed that the height of the water-flowing fractured zone of the experimental working face after SBM was about 103.7 m, which was essentially consistent with the results of the mechanical calculation (106.9 m). This verified the accuracy and reliability of the established mechanical model in this study. In conclusion, SBM not only protects water resources, but also enhances the recovery rate of coal resources, thus providing both economic and environmental benefits.

Supplementary Information The online version contains supplementary material available at https://doi.org/10.1007/s10230-021-00821-y.

Acknowledgements This research was funded by the National Natural Science Foundation of China (52004201, 51874284), China Postdoctoral Science Foundation (2020M683677XB) and Natural Science Foundation of Shaanxi Provincial Department of Education (20JK0765).

References

Bian ZF, Lei SG, Jin D, Wang L (2018) Several basic scientific issues related to mined land remediation. China Coal Soc 43(1):190–197. https://doi.org/10.13225/j.cnki.jccs.2017.4004 (**in Chinese, with English abstract**)

Chi MB, Zhang DS, Fan GW, Zhang W, Liu HL (2019) Prediction of water resource carrying capacity by the analytic hierarchy process-fuzzy discrimination method in a mining area. Ecol Indic 96:647–655. https://doi.org/10.1016/j.ecolind.2018.09.021

Deng XJ, Yuan ZX, Li Y, Liu H, Feng JY, de Wit B (2020) Experimental study on the mechanical properties of microbial mixed backfill. Constr Build Mater 265:120643. https://doi.org/10.1016/j.conbuildmat.2020.120643

Fan LM (2017) Scientific connotation of water-preserved mining. China Coal Soc 45(1):27–35. https://doi.org/10.13225/j.cnki.jccs.2017.5066 (**in Chinese, with English abstract**)

Fan LM (2018) Some scientific issues in water-preserved coal mining. China Coal Soc 44(3):667–674. https://doi.org/10.13225/j.cnki.jccs.2018.6051 (**in Chinese, with English abstract**)

Fan LM, Ma XD, Ji RJ (2015) Progress in engineering practice of water-preserved coal mining in western eco-environment frangible area. China Coal Soc 40(8):1711–1717. https://doi.org/10.13225/j.cnki.jccs.2015.0223 (**in Chinese, with English abstract**)

Hu ZQ, Xiao W, Zhao YL (2020) Re-discussion on coal mine eco-environment concurrent mining and reclamation. China Coal Soc 45(1):351–359. https://doi.org/10.13225/j.cnki.jccs.YG19.1694 (**in Chinese, with English abstract**)

Huang YL, Zhang JX, Zhang Q, Nie SJ, An BF (2012) Strata movement control due to bulk factor of backfilling body in fully mechanized backfilling mining face. J Min Saf Eng 29(2):162–167. https://doi.org/10.3969/j.issn.1673-3363.2012.02.003 (**in Chinese, with English abstract**)

Huang YL, Li JM, Song TQ, Kong GQ, Li M (2017) Analysis on filling ratio and shield supporting pressure for overburden movement control in coal mining with compacted backfilling. Energies 10(1):31. https://doi.org/10.3390/en10010031

Huang P, Spearing S, Ju F, Jessu KV, Wang ZW, Ning P (2019) Control effects of five common solid waste backfilling materials on in situ strata of gob. Energies 12(1):154. https://doi.org/10.3390/en12010154

Huang YL, Li JM, Ma D, Gao HD, Guo YC, Ouyang SY (2020) Triaxial compression behaviour of gangue solid wastes under effects of particle size and confining pressure. Sci Total Environ 693:133607. https://doi.org/10.1016/j.scitotenv.2019.133607

Ju JF, Li QS, Xu JL, Wang XZ, Lou JF (2020) Self-healing effect of water-conducting fractures due to water-rock interactions in undermined rock strata and its mechanisms. Bull Eng Geol Environ 79(1):287–297. https://doi.org/10.1007/s10064-019-01550-x

Li JM (2021) 3D fabric spatiotemporal evolution characteristics and transparent characterization of gangue solid waste backfilling material during compression. Diss, China Univ of Mining & Technology (**in Chinese**)

Li M, Zhang JX, Jiang HQ, Huang YL, Zhang Q (2014) A thin plate on elastic foundation model of overlying strata for dense solid backfill mining. J China Coal Soc 39(12):2369–2373. https://doi.org/10.13225/j.cnki.jccs.2013.1843 (**in Chinese, with English abstract**)

Li M, Zhang JX, Huang YL, Zhang Q (2017) Research on compression ratio design based on compaction properties of solid backfill materials. J Min Saf Eng 34(6):1110–1115. https://doi.org/10.13545/j.cnki.jmse.2017.06.011 (**in Chinese, with English abstract**)

Liu F, Cao WJ, Zhang JM, Cao GM, Guo LF (2021) Current technological innovation and development direction of the 14th Five-Year Plan period in China coal industry. J China Coal Soc 46(1):1–15. https://doi.org/10.13225/j.cnki.jccs.2016.5045 (**in Chinese, with English abstract**)

Ma LQ, Jin ZY, Liang JM, Sun H, Zhang DS, Li P (2015) Simulation of water resource loss in short-distance coal seams disturbed by repeated mining. Environ Earth Sci 74(7):5653–5662. https://doi.org/10.1007/s12665-015-4581-6

Miao XX, Zhang JX, Guo GL (2010) Study on waste-filling method and technology in fully-mechanized coal mining. China Coal Soc 35(1):1–6. https://doi.org/10.13225/j.cnki.jccs.2010.01.006 (**in Chinese, with English abstract**)

Miao XX, Cui XM, Wang JA, Xu JL (2011) The height of fractured water-conducting zone in undermined rock strata. Eng Geol 120(1):32–39. https://doi.org/10.1016/j.enggeo.2011.03.009

Ministry of Emergency Management of the People's Republic of China (2017) Regulation of coal mining under buildings, railways and water bodies. China Coal Industry Publishing House Press, Beijing (**in Chinese**)

Pu H (2008) Structural motion of water-resisting key strata lying on overburden. Int J Min Sci Technol 18(3):353–357. https://doi.org/10.1016/S1006-1266(08)60074-7

Pu H (2010) Study on the theory and application of water-resisting key strata on water-preserved mining. Diss, China Univ of Mining & Technology (**in Chinese**)

Qi WY, Huang YL, He H, Zhang JX, Li JM, Qiao M (2019) Potential pollution of groundwater by dissolution and release of contaminants due to using gangue for backfilling. Mine Water Environ 38(2):281–293. https://doi.org/10.1007/s10230-018-00585-y

Scheiber L, Ayora C, Vazquez-Sune E (2018) Quantification of proportions of different water sources in a mining operation. Sci Total Environ 619:287–599. https://doi.org/10.1016/j.scitotenv.2017.11.172

Selvadurai APS, Gladwell GML (1979) Elastic analysis of soil-foundation interaction. Eng Geol 17(1):71–75. https://doi.org/10.1115/1.3153622

Shan PF, Lai XP, Liu XM (2020) An associated evaluation methodology of initial stress level of coal-rock masses in steeply inclined coal seams, Urumchi coal field, China. Eng Comput 37(6):2177–2192. https://doi.org/10.1108/EC-07-2019-0325

Sun Q, Zhang JX, Zhang S, Yin W, Zhou N, Liu Y (2017) Study of stability of surrounding rock and characteristic of overburden strata movement with longwall roadway backfill coal mining. China Coal Soc 42(2):404–412. https://doi.org/10.13225/j.cnki.jccs.2016.6019 (**in Chinese, with English abstract**)

Xu JL, Wang XZ, Liu WT, Wang ZG (2009) Effects of primary key stratum location on height of water flowing fracture zone. J Rock Mech Eng 28(2):380–385. https://doi.org/10.13225/j.cnki.jrme.0.2009-02-026 (**in Chinese, with English abstract**)

Xu JL, Zhu WB, Wang XZ (2012) New method to predict the height of fractured water-conducting zone by location of key strata. China Coal Soc 37(5):762–769. https://doi.org/10.13225/j.cnki.jccs.2012.05.002 (**in Chinese, with English abstract**)

Yan H, Zhang JX, Zhou N, Zhang S, Dong XJ (2018) Shaft failure characteristics and the control effects of backfill body

compression ratio at ultra-contiguous coal seams mining. Environ Earth Sci 77(12):458. https://doi.org/10.1007/s12665-018-7641-x

Yan H, Zhang JX, Zhang S, Zhang S, Zhou N (2019) Physical modeling of the controlled shaft deformation law during the solid backfill mining of ultra-close coal seams. Bull Eng Geol Environ 78(5):3741–3754. https://doi.org/10.1007/s10064-018-1335-1

Yu YX, Huang RB, Wang BQ (2016) Analysis on limit equilibrium zone of coal pillar in mining roadway based on mechanical model of elastic foundation beam. J Eng Mech 142(4):04016009. https://doi.org/10.1061/(ASCE)EM.1943-7889.0001032

Zhang Y (2019) The mechanism of developmental behavior of water-conducting fracture in the overlying strata of short-wall block mining and the control technology. Diss, China Univ of Mining & Technology (**in Chinese**)

Zhang JC, Shen BH (2004) Coal mining under aquifers in China: a case study. Int J Rock Mech Min Sci 41:629–639. https://doi.org/10.1016/j.ijrmms.2003.01.005

Zhang DS, Fan GW, Liu YD, Ma LQ (2010) Field trials of aquifer protection in longwall mining of shallow coal seams in China. Int J Rock Mech Min Sci 47(6):908–914. https://doi.org/10.1016/j.ijrmms.2010.06.018

Zhang DS, Fan GW, Ma LQ, Wang XF (2011) Aquifer protection during longwall mining of shallow coal seams: a case study in the Shendong coalfield of China. Int J Coal Geol 86:190–196. https://doi.org/10.1016/j.coal.2011.01.006

Zhang JX, Jiang HQ, Deng XJ, Ju F (2014) Prediction of the height of the water-conducting zone above the mined panel in solid backfill mining. Mine Water Environ 33(4):317–326. https://doi.org/10.1007/s10230-014-0310-8

Zhang JX, Zhang Q, Sun Q, Gao R, Germain D, Abro S (2015) Surface subsidence control theory and application to backfill coal mining technology. Environ Earth Sci 74(2):1439–1448. https://doi.org/10.1007/s12665-015-4133-0

Zhang JX, Li BY, Zhou N, Zhang Q (2016) Application of solid backfilling to reduce hard-roof caving and longwall coal face burst potential. Int J Rock Mech Min Sci 88:197–205. https://doi.org/10.1016/j.ijrmms.2016.07.025

Zhang DS, Li WP, Lai XP, Fan GW, Liu WQ (2017a) Development on basic theory of water protection during coal mining in northwest in China. J China Coal Soc 42(1):36–43. https://doi.org/10.13225/j.cnki.jccs.2016.5045 (**in Chinese, with English abstract**)

Zhang JX, Huang P, Zhang Q, Li M, Chen ZW (2017b) Stability and control of room mining coal pillars-taking room mining coal pillars of solid backfill recovery as an example. J Cent South Univ 24(5):1121–1132. https://doi.org/10.1007/s11771-017-3515-8

Zhang Y, Cao SG, Guo S, Wan T, Wang JJ (2018) Mechanisms of the development of water-conducting fracture zone in overlying strata during shortwall block backfill mining: a case study in northwestern China. Environ Earth Sci 77(14):543. https://doi.org/10.1007/s12665-018-7726-6

Zhang JX, Sun Q, Li M, Zhao X (2019) The mining-induced seepage effect and reconstruction of key aquiclude strata during backfill mining. Mine Water Environ 38(3):590–601. https://doi.org/10.1007/s10230-019-00614-4

Zhang Y, Cao SG, Zhang N, Zhao CZ (2020) The application of short-wall block backfill mining to preserve surface water resources in northwest China. J Clean Prod 261:121232. https://doi.org/10.1016/j.jclepro.2020.121232

Zhou N, Yao YN, Song WJ, He ZW, Meng GH, Liu Y (2020) Present situation and prospect of coal gangue treatment technology. J Min Saf Eng 37(1):136–146. https://doi.org/10.13545/j.cnki.jmse.2020.01.015 (**in Chinese, with English abstract**)